Solid-State, Polymer-Based Fiber Solar Cells with Carbon Nanotube Electrodes

Dianyi Liu,[†] Mingyan Zhao,[†] Yan Li,[†] Zuqiang Bian,[†,*] Luhui Zhang,[‡] Yuanyuan Shang,[‡] Xinyuan Xia,[†] Sen Zhang,[†,§] Daqin Yun,[†] Zhiwei Liu,[†] Anyuan Cao,[‡,*] and Chunhui Huang[†]

[†]Beijing National Laboratory for Molecular Sciences, State Key Laboratory of Rare Earth Materials Chemistry and Applications, College of Chemistry and Molecular Engineering, Peking University, Beijing 100871, People's Republic of China, [‡]Department of Materials Science and Engineering, College of Engineering, Peking University, Beijing 100871, People's Republic of China, and [§]Department of Energy and Resources Engineering, College of Engineering, Peking University, Beijing 100871, People's Republic of China

ABSTRACT Most previous fiber-shaped solar cells were based on photoelectrochemical systems involving liquid electrolytes, which had issues such as device encapsulation and stability. Here, we deposited classical semiconducting polymer-based bulk heterojunction layers onto stainless steel wires to form primary electrodes and adopted carbon nanotube thin films or densified yarns to replace conventional metal counter electrodes. The polymer-based fiber cells with nanotube film or yarn electrodes showed power conversion efficiencies in the range 1.4% to 2.3%, with stable performance upon rotation and large-angle bending and during long-time storage without further encapsulation. Our fiber solar cells consisting of a polymeric active layer sandwiched between steel and carbon electrodes have potential in the manufacturing of low-cost, liquid-free, and flexible fiber-based photovoltaics.

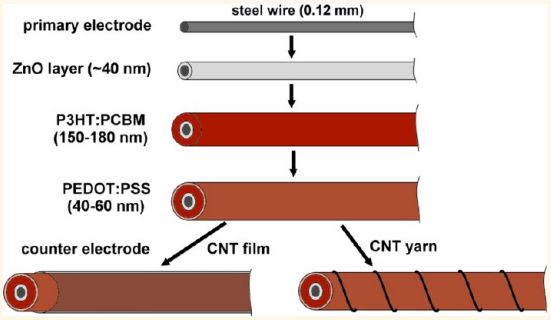

KEYWORDS: fiber solar cell · semiconducting polymer · carbon nanotube

Fiber solar cells (FSCs) are promising candidates for making flexible, scalable, large-area power supply electronics in the form of woven fabrics or mats.[1−5] Various FSCs have been reported during the past years, and those devices generally can be divided into two types based on materials involved and charge transport mechanism. One type was based on photoelectrochemical systems consisting of dye-sensitized TiO_2 nanoparticles or nanotubes,[6−11] semiconducting nanowire (*e.g.*, CdSe) arrays,[12,13] and quantum dot-sensitized ZnO nanowires.[14,15] Photoelectrochemical FSCs have been extensively studied and showed advantages such as high power conversion efficiency (4−7%) and reliable fabrication processes.[7,10] However, involvement of a liquid electrolyte also posed great challenges in device encapsulation for practical applications. Some FSCs had to be encapsulated and tested within a transparent glass tube (holding the electrolyte); thereby device flexibility was reduced.[6,8,11] Recently, solid electrolyte (CuI) TiO_2-based dye-sensitized fiber cells with an efficiency of 1.38% were reported.[16]

The second type of FSCs were based on solid-state organic active layers, which were much less studied compared to dye-sensitized structures.[1,17,18] A few other reports evaporated metal electrodes on the polymer layers, and incident light had to be directed into the FSC through an optical fiber inside.[19−22] Organic solar cells (OSCs) offer an alternative approach toward low-cost, moderate-efficiency, third-generation photovoltaics.[23] Efficiencies of planar OSCs based on polymeric molecules with specially designed structures and band gaps, or in a tandem junction, have been continuously improved to about 8% in recent times.[24,25] Semiconducting polymers can be processed in solution and coated to various substrates including thin fibers and wires; therefore polymeric materials are compatible with the fabrication and functionality of FSCs. At the same time, many metals or nanostructures (*e.g.*, Ag nanowires, carbon nanotubes, graphene) can be coated on polymer layers as electrical contacts, offering good choices as primary and counter electrodes for polymer-based FSCs.[26−29] Despite these promising aspects, there have been very few reports on organic FSCs possibly

* Address correspondence to bianzq@pku.edu.cn, anyuan@pku.edu.cn.

Received for review October 6, 2012 and accepted November 5, 2012.

Published online November 05, 2012
10.1021/nn304638z

because the polymer-coating process on fiber or wire surfaces is difficult to control compared to spin-coating a film on planar substrates, and twisting of a rigid metal wire electrode could easily penetrate thin polymer layers (causing a short circuit). Therefore, it is critical to explore suitable counter electrode materials and structures that can be applied to wire-supported polymer layers conveniently while maintaining device flexibility. Here, we show that carbon nanotube (CNT) films and yarns, which have already been used as electrodes for various planar solar cells and photoelectrochemical FSCs,[12,13,30−34] are also suitable for creating flexible and stable polymer-based FSCs.

RESULTS AND DISCUSSION

Our polymer FSCs were fabricated by dip-casting multiple functional layers sequentially on the surface of stainless steel wires (0.12 mm in diameter) (see Methods), as illustrated in Figure 1. The first layer of ZnO nanocrystals (40 nm thick) synthesized on the wire surface served as a hole-blocking layer and also a transitional layer to facilitate adhesion of polymer layers in subsequent steps. A classical bulk heterojunction layer of poly(3-hexylthiophene) (P3HT) and [6,6]-phenyl-C_{61}-butyric acid methyl ester (PCBM) (weight ratio 1:0.8) was casted onto the ZnO layer by repeated solution dipping and thermal annealing to render an appropriate thickness in the range 150−180 nm. On top of the P3HT, a poly(3,4-ethylene-dioxythiophene): poly(styrenesulfonate) (PEDOT:PSS) layer (40 to 60 nm in thickness) was dip-casted to improve hole transport and electrical contact to the counter electrode. Single-walled CNT films and spun yarns were explored here as counter electrodes. The CNT film was wrapped around the core wire as a transparent conductive electrode, whereas the yarn was twisted in a way similar to traditional metal wires. The resulting coaxial structure was a steel wire-sustained ZnO-P3HT:PCBM-PEDOT triple layer with controlled layer thicknesses and lengths along the wire, which are then covered (or twisted) by a CNT film/yarn. This configuration also could be seen as an organic active layer sandwiched between a low-cost primary electrode (steel wire) and a CNT-based counter electrode, with two additional layers (ZnO and PEDOT) to improve charge transport and maintain good contact to the electrodes.

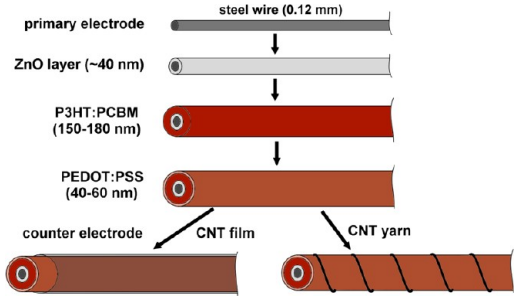

Figure 1. Illustration of the fiber-shaped solar cell structure and fabrication process. The primary electrode is a stainless steel wire (0.12 mm in diameter), which is coated by a ZnO layer (thickness of ~40 nm), a P3HT:PCBM bulk heterojunction layer (150−180 nm in thickness), and a PEDOT:PSS layer (40−60 nm in thickness) in sequence. After that, a transparent conductive CNT film was wrapped onto the polymer layer as the counter electrode, or in another configuration, a CNT yarn (spun from the film) was twisted around the core wire.

We have performed scanning electron microscopy (SEM) characterization on the wire structure at different stages during fabrication. The ZnO coating was obtained by dipping a certain wire length into its precursor solution and then converting to nanocrystals by thermal annealing (Figure 2a). The ZnO coating was macroscopically continuous, but at microscale it was

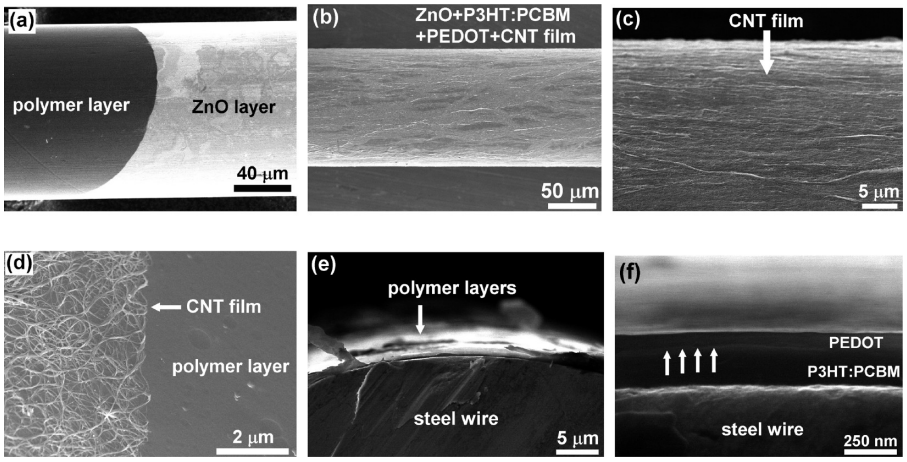

Figure 2. Characterization of polymer FSCs with a CNT film as counter electrode. (a) SEM image of a steel wire coated by a ZnO layer (right side) and polymer layers (P3HT:PCBM and PEDOT) (left side). (b) Freestanding wire coated with ZnO, P3HT:PCBM, and PEDOT multilayers and wrapped by a CNT film. (c) SEM image of the CNT film coated on the wire surface. (d) Enlarged view at the interface showing the CNT network and the underlying polymer layer. (e) Cross-sectional SEM image of the wire showing the polymer layers coated on the wire surface. Part of the polymer layer near the edge was detached from the substrate due to the cutting process to expose the cross section. (f) Cross-sectional SEM image of the polymer coating showing a PEDOT layer stacked on a P3HT:PCBM layer. Vertical arrows indicate the interface between the P3HT and PEDOT layers.

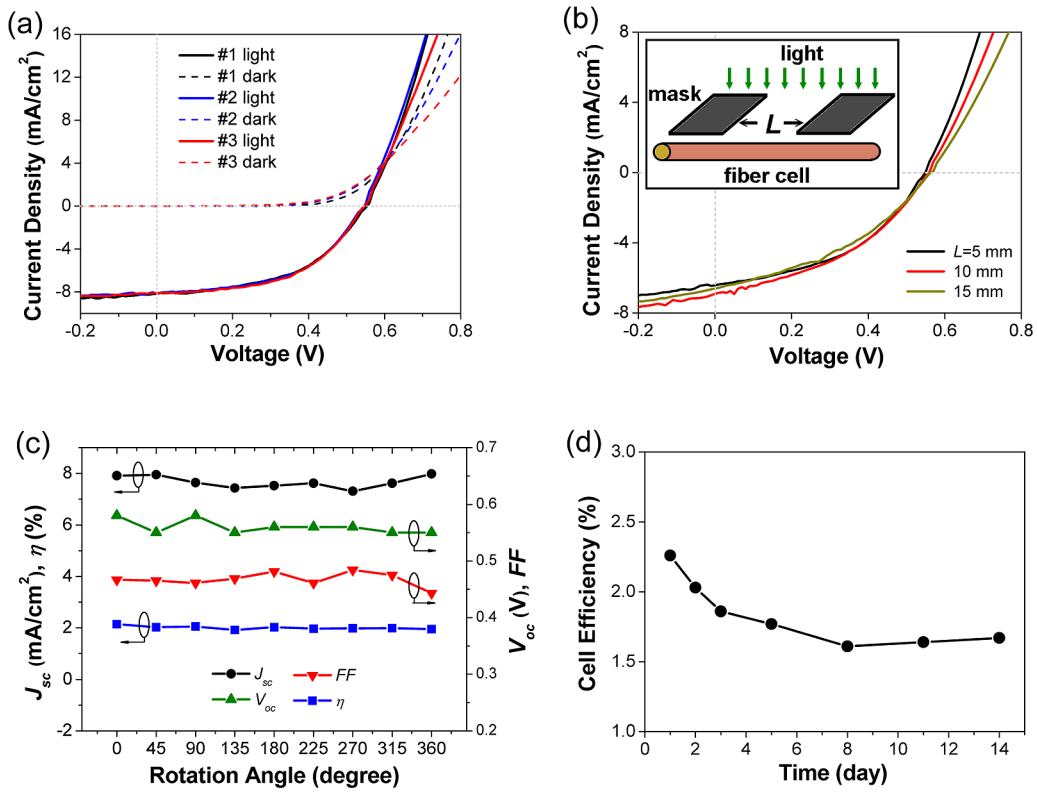

Figure 3. *J*−*V* **characteristics of polymer-based FSCs with CNT film counter electrode. (a) Dark and light** *J*−*V* **curves of three good polymer FSCs with similar behavior and cell efficiencies of 2.26% (for sample #1), 2.31% (for #2), and 2.29% (for #3), respectively. (b)** *J*−*V* **curves of a FSC illuminated over different wire lengths (*L* = 5, 10, 15 mm, respectively). Inset shows the illumination setup in which *L* is defined by a mask. (c) Rotation tests including typical cell parameters (J_{sc}, V_{oc}, FF, η) recorded during steel wire rotation from 0° to 360°. (d) Measured cell efficiencies in an uncapsulated FSC during storage in inertial gas for a period of 14 days.**

made of nanocrystal aggregations with sizes of 20−40 nm. This surface morphology was favorable for subsequent solution casting of polymers such that more solution could be retained by a rough nanocrystal layer. Figure 2b showed a freestanding wire coated by multiple functional layers including a P3HT:PCBM layer, a PEDOT layer, and a CNT film from inside to outside. The CNT film wrapped around the core wire tightly, enabled by ethanol wetting and evaporation, which collapsed the film onto the wire surface (Figure 2c). From the film edge we observed a network of small CNT bundles well adhered on the polymer layer, forming good contact (Figure 2d). As a transparent conductive electrode, the CNT film ensured 100% surface coverage on the active layer, which was favorable for efficient charge extraction and collection from underlying polymers.

To view the thicknesses of the polymer layers, we cut the steel wire in the middle to expose the cross section. Figure 2e shows that the polymer layers coated on the wire surface could be distinguished clearly. The enlarged view revealed very uniform polymer coatings consisting of a P3HT:PCBM layer (about 150 nm in thickness) at the bottom and a PEDOT layer (~60 nm) stacked on the top, with a clear interface between the two layers (Figure 2f). The bulk heterojunction thickness was controlled in this range to ensure maximum optical absorption and cell efficiency. SEM results indicated that our methods had led to continuous and uniform polymer layers on the primary electrode, which was an essential step for fabrication of fiber solar cells.

We have characterized current density−voltage (*J*−*V*) curves of the polymer FSCs with CNT film counter electrodes under standard illumination conditions (air mass 1.5, calibrated intensity = 100 mW/cm^2). Two terminals were made by contacting one end of the CNT film by Ag paste and the other end of the primary electrode (exposed section of the steel wire) for electrical connection. Incident light was directed to the freestanding cells through a shadow mask placed at the front of the wire to define an illumination length (*L*) along the wire axis. The three most efficient samples made by our process showed reproducible behavior with an open-circuit voltage (V_{oc}) of 0.55 V, a short-circuit current density (J_{sc}) of about 8.1 mA/cm^2, a fill factor (FF) of more than 50%, and very similar power conversion efficiencies (η) of 2.26−2.31%. In the dark, all samples exhibited typical diode properties. This efficiency was close to the planar solar cell with the same active layer (P3HT:PCBM) and CNT film electrode (η = 2.48%) reported recently.[26] Here, the results were

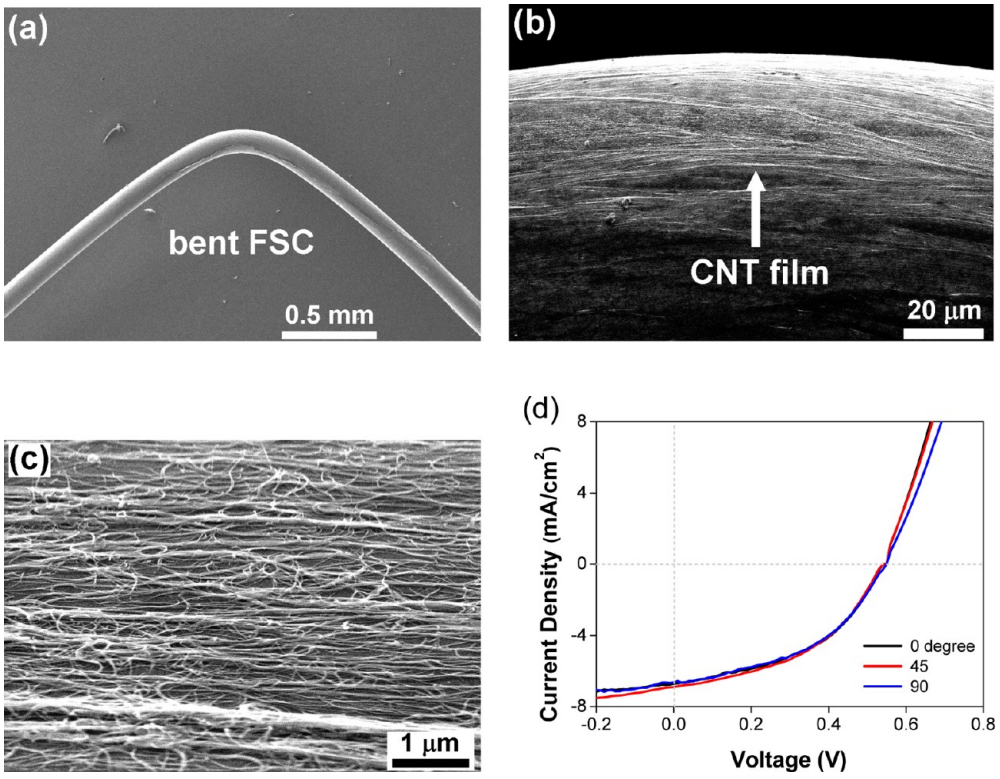

Figure 4. Bending flexibility of polymer FSCs with CNT film electrodes. (a) SEM image of fiber cells bent to nearly 90 degrees. (b) Close view of the bent region at the curvature showing that the CNT film covered on the wire remains continuous (without breaking). (c) Enlarged view of the CNT film showing that the CNT network has been slightly stretched along the wire axis direction. (d) *J*–*V* curves of a FSC in straight form (0 degree) and bent to 45 and 90 degrees, respectively, showing stable behavior during bending.

based on optimized polymer layer thicknesses that were in the range 150–180 nm for the P3HT:PCBM layer and 40–60 nm for the PEDOT layer. When the P3HT:PCBM thickness was decreased to <100 nm or increased to >200 nm, the cell efficiencies quickly dropped to about 1% in both cases due to a simultaneous decrease in V_{oc} and J_{sc}.

We also tested the FSCs by changing the illumination lengths from 5 to 15 mm. We found that the V_{oc} remained stable (0.55 to 0.56 V) while the J_{sc} varied from 6.43 to 6.91 mA/cm^2 and the efficiency decreased slightly from 1.58% to 1.45% with increasing the length to 15 mm (Figure 3b). At increasing working length, charge carriers (holes) must travel a longer distance through the CNT film to be collected, resulting in a drop of the fill factor from 45% to 39%. The degradation of efficiency was less than 10% when the illumination region increased by 3-fold, a promising aspect for scalable production of longer FSCs while maintaining cell efficiency. Also, because the wire was wrapped by the transparent CNT film uniformly along the circumference, the FSC could be rotated without light blocking, as possibly occurred in a twisted double-wire configuration. Key parameters including J_{sc}, V_{oc}, FF, and η showed very small fluctuations during rotation of the steel wire over 360 degrees (one cycle) (Figure 3c). In particular, the cell efficiency was stabilized at about 2% (from 1.92% to 2.14%) during the entire rotation process. Compared to photoelectrochemical fiber cells, in which the liquid electrolyte might flow during rotation and cause variation in device performance, our solid-state FSCs ensured high stability due to uniform CNT film coverage and absence of electrolyte.

Stability over long-time storage is an important issue for organic solar cells because of the degradation of polymers induced by many factors such as the presence of oxygen and moisture in air. We have stored a FSC in a glovebox (nitrogen atmosphere) and monitored the cell performance over a period of 14 days. The cell efficiency dropped quickly from 2.26% down to 1.77% in the initial 5 days and then stabilized at about 1.6–1.7% in the later stage (Figure 3d). The drop of efficiency was mainly due to a continuous decrease of J_{sc} (from 8.2 to 7.4 mA/cm^2) and FF (from 50% to 42%) over time. Here, the stability tests were carried out on a directly exposed FSC without further encapsulation. In this case, the CNT film on the polymer layer also could help protect the device by blocking foreign molecules to some degree. In addition, we measured the cell stability during storage in an ambient atmosphere of two FSCs with a CNT film (or yarn) electrode and found that the degradation in air was faster than in nitrogen (Supporting Information, Figure S1).

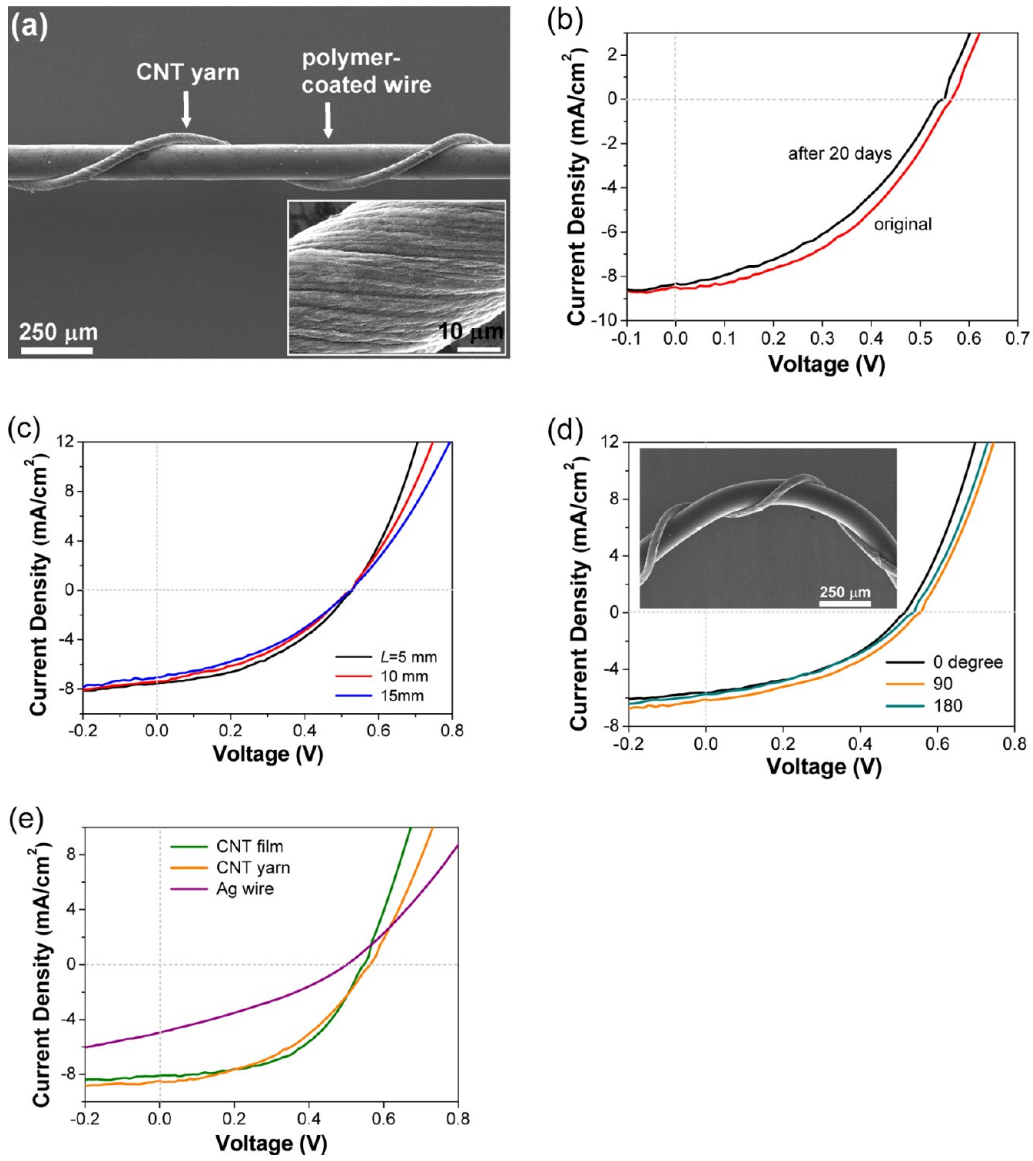

Figure 5. Characterization of polymer-based FSCs with CNT yarn counter electrodes. (a) SEM image of a polymer FSC twist by a CNT yarn electrode. Inset shows the close view of the yarn. (b) *J*–*V* characteristics of a FSC in original state and after storage in inertia gas for 20 days. (c) *J*–*V* curves of a FSC with different illumination lengths (*L* = 5, 10, 15 mm, respectively). (d) *J*–*V* curves of a FSC in straight form (0 degree) and bent to 90 and 180 degrees, respectively. Inset shows the SEM image of the FSC twisted by a CNT yarn electrode and bent to 90 degrees. (e) *J*–*V* curves of polymer FSCs with different counter electrodes including a CNT film, a CNT yarn, and a Ag wire with similar diameter, respectively.

Our polymer FSCs were highly flexible and could be bent to large angles without efficiency degradation. SEM characterization allowed direct imaging of a bending wire (bent to 90 degrees) and the morphology of CNTs on it (Figure 4a). In the curved region, the CNT film remained continuous and well adhered to the wire substrate (Figure 4b). This result highlighted the advantages of using highly flexible and soft CNT films compared to (usually brittle) metal films. Moreover, the CNT network had been slightly stretched along the wire length due to the tensile strain produced on the outside of the bent wire (Figure 4c). Thus the deformability of our CNT films prevented cracking in the curved area and enabled the FSCs to work at large bending angles and under tension. The *J*–*V* characteristics were very stable upon bending to 45 and 90 degrees compared to the straight form (Figure 4d). The V_{oc} values were 0.54 to 0.55 V, while the efficiencies were 1.65% to 1.68%, indicating very small fluctuation when the steel wire was deformed in this way. CNT films have been used as flexible electrodes for planar solar cells fabricated on plastic substrates previously, and here they were also very suitable to construct flexible fiber solar cells.

Furthermore, we also constructed polymer FSCs with CNT yarn (*versus* film) electrodes. The CNT yarn (60 μm in diameter) was spun from a sheet of as-synthesized CNT film and then twisted along the steel

wire at controlled pitch (2 mm) (Figure 5a). In this configuration, the CNT yarn resembled metal (*e.g.*, Pt) wires used in previous fiber cells but with better flexibility. Compared to the CNT film, which covers the entire cell surface, the yarn only contacted a small fraction of the polymer layer. However, because of the densification of CNTs caused by twist-spinning (inset of Figure 5a), the yarn conductivity had been significantly increased, which was a favorable factor for charge collection. Therefore a CNT yarn as counter electrode had less surface coverage on polymers but improved conductivity. A typical FSC with a yarn electrode showed a V_{oc} of 0.56 V, a J_{sc} of 8.49 mA/cm^2, and η of 2.11% (Figure 5b), comparable to the efficiency obtained in the FSC using a film electrode (2.31%). The same device retained an efficiency of 1.86% after 20 days' storage in inertial gas (Figure 5b). We have changed the yarn twisting pitch from 2 mm down to 0.5 mm in the same FSC and obtained similar $J-V$ curves and cell efficiencies, indicating that within a certain range the surface coverage by counter electrodes did not have a significant influence on the cell performance (Figure S2). This result was very encouraging, as the use of both CNT films and yarns could enable different electrode configurations and greatly extend the versatility of our polymer FSCs.

In addition, we have tested the length dependence of the cell performance. The J_{sc} value decreased from 7.6 to 7.1 mA/cm^2 when the illumination length increased from 5 to 15 mm, while the V_{oc} remained constant (0.55 V), resulting in a modest degradation of cell efficiency from 1.68% to 1.42% (Figure 5c). We suppose that further optimization of the yarn diameter and conductivity could limit the efficiency degradation at increasing wire length. Similar to a CNT film-wrapped wire, a yarn-twisted FSC showed high stability during bending to 90 and 180 degrees (Figure 5d). The SEM image showed a FSC with a CNT yarn in twisted state (inset of Figure 5d). The slight fluctuation of cell parameters might be due to the contact variation between the yarn and bending wire at different angles.

Finally, we compared the CNT film and yarn to a metal wire as counter electrode. A control sample was made by twisting a Ag wire with similar diameter (100 μm) to the polymer-coated primary electrode and tested it under the same conditions. The FSC with Ag wire electrode showed a reduced V_{oc} of 0.50 V, a J_{sc} of 5.0 mA/cm^2, and an efficiency of 0.8%, which was lower than the FSCs with CNT film/yarn electrodes (>2%) (Figure 5e). Compared to a flexible CNT film/yarn, it was more difficult to twist the relatively rigid Ag wire along the steel wire to form a nice and conformal contact yet without penetrating the thin polymer layer. The above results indicated that both CNT films and yarns are suitable electrode materials for fiber cells, with additional advantages such as a more controllable fabrication process and improved cell efficiency.

CONCLUSION

In conclusion, we demonstrated polymer FSCs consisting of a uniform P3HT:PCBM coating on steel wires and measured power conversion efficiencies of more than 2%. We adopted single-walled CNTs in different morphologies such as semitransparent thin films or densified spun yarns to serve as counter electrodes and, more importantly, to improve the device versatility. Compared to noble metal wires frequently used in fiber cells, the CNT films and yarns have the potential to reduce the device weight/size, lower the cost of electrode materials, and enhance device flexibility. Other semiconducting polymers developed recently might also be applied to our model to fabricate solid-state fiber solar cells with high efficiency. Improved techniques for producing large-size, high-conductivity, freestanding CNT films that could be easily applied to fiber substrates may enable scalable production of efficient fiber solar cells.

METHODS

1. Synthesis of CNT Films and Yarns. Single-walled CNT films were prepared by a chemical vapor deposition (CVD) process using xylene and ferrocene as carbon source and catalyst precursor, respectively. Ferrocence was dissolved into xylene at a concentration of 0.06 g/mL and then mixed with sulfur powders to form a suspension (Fe/S ratio of 10:1). The suspension was injected into a quartz tube housed in the CVD furnace at a rate of 2−4 μL/min under argon (2500 sccm) and hydrogen (400 sccm) flow. The reaction temperature was set as 1160 °C, and the typical period was 40 min. Spiderweb-like CNT films were grown in the vapor phase, carried by the Ar/H_2 gas to the downstream zone, and deposited on a nickel foil substrate placed there. To spin the yarn, a purified CNT film immersed in ethanol was picked up and shrunk into a thin shred during ethanol evaporation. Two ends of this film were fixed on the rotating shafts of two electric motors and spun for 5 min at a constant speed of 27 rpm; after that the film was twisted into a highly densified yarn. Typically, the areas of as-synthesized films were 10−100 cm^2 and the yarns had diameters of 50−100 μm and lengths up to several cm.

2. Fabrication of the Fiber Solar Cells. Solar cells were fabricated on commercial stainless steel wires (purchased from Alfa Aesar, 0.127 mm in diameter, type 304). Multiple functional layers were prepared in sequence by the dip-coating method with a coating speed of about 10 mm s^{-1}. First, the ZnO precursor layer was applied onto the precleaned surface of a stainless steel wire by immersing the wire into a zinc acetate−ethanol amine in 2-methoxyethanol solution. Then the layer was converted into ZnO nanocrystals by thermal annealing at 300 °C for 60 min in air, and this procedure was repeated three times to obtain a continuous nanocrystal film with appropriate thickness (~40 nm). Second, a chlorobenzene solution of P3HT (Regioregular, Rieke Metals) (30 mg/mL) and PCBM (>99%, Sigma-Aldrich) (24 mg/mL) was dip-coated on the wire with a ZnO layer in a glovebox and annealed at 150 °C for 10 min to form a uniform polymer bulk heterojunction layer on top of ZnO. After that, the wire surface was deposited by a diluted PEDOT:PSS solution in 2-propanol at 80 °C and annealed at

150 °C for 10 min. For devices using a CNT film as counter electrode, a CNT film was picked up from Ni foil after CVD and directly wrapped on the polymer-coated wire surface. Then a droplet of ethanol was delivered to the wire surface to let the CNT film collapse onto the polymer layers by ethanol wetting and subsequent evaporation. The wire was dried in N_2 to form a good contact between the CNT film and the polymer. For devices using CNT yarn as counter electrode, a 3−4 cm long, 50−80 μm diameter yarn was twisted around the polymer−steel wire at a set pitch of 2 mm and fixed at the ends. As a control sample, a Ag wire (purchased from Alfa Aesar, 0.1 mm in diameter) was twisted onto the polymer−steel wire with the same pitch. For making an electrical connection, one exposed end of the steel wire (without polymer coating) was connected as a negative terminal and the other end of the CNT film (or CNT yarn) was connected as a positive terminal by Ag paste. All fiber solar cells were freestanding and tested without further encapsulation.

3. Characterization and Solar Cell Measurement. The morphology and structure of the steel wires, ZnO and polymer coatings, and CNT films/yarns were characterized by SEM images using a Hitachi S-4800 cold field emission scanning microscope. The current−voltage curves of the solar cells were measured by a Keithley 4200 semiconductor characterization system and illuminated by an Oriel 300 W solar simulator (Thermo Oriel 91160-1000) with an AM 1.5 G filter at a calibrated intensity of 100 mW/cm^2, determined by a standard silicon solar cell. The irradiated length of the fiber cells was defined by a photomask, and the irradiated area of the cells was taken as this length multiplied by the wire diameter after polymer coating. Current density values were calculated based on the above cell area. For rotation tests, the fiber cell was fixed at one end and rotated around its axis intermittently to predefined angles. For bending tests, the fiber cell was also fixed at one end and bent manually at the other end to desired angles by a tweezer. For stability tests, the fiber cell was stored in a glovebox (N_2 atmosphere) for specific times and then taken out to measure the performance in ambient environment.

Conflict of Interest: The authors declare no competing financial interest.

Acknowledgment. The authors are grateful to the National Basic Research Program (2011CB933303) and the National Natural Science Foundation (NSFC) of China (90922004) for financial support. A.C. acknowledges financial support by the NSFC program (grant no. 51072005).

Supporting Information Available: This material is available free of charge *via* the Internet at http://pubs.acs.org.

REFERENCES AND NOTES

1. Lee, M. R.; Eckert, R. D.; Forberich, K.; Dennler, G.; Brabec, C. J.; Gaudiana, R. A. Solar Power Wires Based on Organic Photovoltaic Materials. *Science* **2009**, *324*, 232–235.
2. Huang, S.; Zhang, Q.; Huang, X.; Guo, X.; Deng, M.; Li, D.; Luo, Y.; Shen, Q.; Toyoda, T.; Meng, Q. Fibrous CdS/CdSe Quantum Dot Co-Sensitized Solar Cells Based on Ordered TiO_2 Nanotube Arrays. *Nanotechnology* **2010**, *21*, 375201.
3. Zou, D.; Wang, D.; Chu, Z.; Lv, Z.; Fan, X. Fiber-shaped Flexible Solar Cells. *Coord. Chem. Rev.* **2010**, *254*, 1169–1178.
4. Pan, C.; Guo, W.; Dong, L.; Zhu, G.; Wang, Z. L. Optical Fiber-Based Core-Shell Coaxially Structured Hybrid Cells for Self-Powered Nanosystems. *Adv. Mater.* **2012**, *24*, 3356–3361.
5. Wang, W.; Zhao, Q.; Li, H.; Wu, H.; Zou, D.; Yu, D. Transparent, Double-Sided, ITO-Free, Flexible Dye-Sensitized Solar Cells Based on Metal Wire/ZnO Nanowire Arrays. *Adv. Funct. Mater.* **2012**, *22*, 2775–2782.
6. Liu, Z. Y.; Misra, M. Dye-Sensitized Photovoltaic Wires Using Highly Ordered TiO_2 Nanotube Arrays. *ACS Nano* **2010**, *4*, 2196–2200.
7. Fu, Y.; Lv, Z.; Hou, S.; Wu, H.; Wang, D.; Zhang, C.; Chu, Z.; Cai, X.; Fan, X.; Wang, Z. L.; *et al*. Conjunction of Fiber Solar Cells with Groovy Micro-Reflectors as Highly Efficient Energy Harvesters. *Energy Environ. Sci.* **2011**, *4*, 3379.
8. Hou, S.; Cai, X.; Fu, Y.; Lv, Z.; Wang, D.; Wu, H.; Zhang, C.; Chu, Z.; Zou, D. Transparent Conductive Oxide-Less, Flexible, and Highly Efficient Dye-Sensitized Solar Cells with Commercialized Carbon Fiber as the Counter Electrode. *J. Mater. Chem.* **2011**, *21*, 13776.
9. Huang, S.; Guo, X.; Huang, X.; Zhang, Q.; Sun, H.; Li, D.; Luo, Y.; Meng, Q. Highly Efficient Fibrous Dye-Sensitized Solar Cells Based on TiO_2 Nanotube Arrays. *Nanotechnology* **2011**, *22*, 315402.
10. Lv, Z.; Fu, Y.; Hou, S.; Wang, D.; Wu, H.; Zhang, C.; Chu, Z.; Zou, D. Large Size, High Efficiency Fiber-Shaped Dye-Sensitized Solar Cells. *Phys. Chem. Chem. Phys.* **2011**, *13*, 10076.
11. Fu, Y.; Lv, Z.; Wu, H.; Hou, S.; Cai, X.; Wang, D.; Zou, D. Dye-Sensitized Solar Cell Tube. *Sol. Energy Mater. Sol. Cells* **2012**, *102*, 212–219.
12. Zhang, L.; Shi, E.; Ji, C.; Li, Z.; Li, P.; Shang, Y.; Li, Y.; Wei, J.; Wang, K.; Zhu, H.; *et al*. Fiber and Fabric Solar Cells by Directly Weaving Carbon Nanotube Yarns with CdSe Nanowire-Based Electrodes. *Nanoscale* **2012**, *4*, 4954.
13. Zhang, L.; Shi, E.; Li, Z.; Li, P.; Jia, Y.; Ji, C.; Wei, J.; Wang, K.; Zhu, H.; Wu, D.; *et al*. Wire-Supported CdSe Nanowire Array Photoelectrochemical Solar Cells. *Phys. Chem. Chem. Phys.* **2012**, *14*, 3583.
14. Chen, H.; Zhu, L.; Wang, M.; Liu, H.; Li, W. Wire-shaped Quantum Dots-Sensitized Solar Cells Based on Nanosheets and Nanowires. *Nanotechnology* **2011**, *22*, 475402.
15. Chen, H.; Zhu, L.; Liu, H.; Li, W. Growth of ZnO Nanowires on Fibers for One-Dimensional Flexible Quantum Dot-Sensitized Solar Cells. *Nanotechnology* **2012**, *23*, 075402.
16. Wang, D.; Hou, S.; Wu, H.; Zhang, C.; Chu, Z.; Zou, D. Fiber-Shaped All-Solid State Dye Sensitized Solar Cell with Remarkably Enhanced Performance *via* Substrate Surface Engineering and TiO_2 Film Modification. *J. Mater. Chem.* **2011**, *21*, 6383.
17. Bedeloglu, A.; Demir, A.; Bozkurt, Y.; Sariciftci, N. S. A Photovoltaic Fiber Design for Smart Textiles. *Text. Res. J.* **2010**, *80*, 1065–1074.
18. O'Connor, B.; Pipe, K. P.; Shtein, M. Fiber Based Organic Photovoltaic Devices. *Appl. Phys. Lett.* **2008**, *92*, 193306.
19. Curran, S.; Talla, J.; Dias, S.; Dewald, J. Microconcentrator Photovoltaic Cell (the m-C Cell): Modeling the Optimum Method of Capturing Light in an Organic Fiber Based Photovoltaic Cell. *J. Appl. Phys.* **2008**, *104*, 064305.
20. Li, Y.; Huang, H. H.; Wang, M. J.; Nie, W. Y.; Huang, W. X.; Fang, G. J.; Carroll, D. L. Spectral Response of Fiber-Based Organic Photovoltaics. *Sol. Energy Mater. Sol. Cells* **2012**, *98*, 273–276.
21. Li, Y. A.; Nie, W. Y.; Liu, J. W.; Partridge, A.; Carroll, D. L. The Optics of Organic Photovoltaics: Fiber-Based Devices. *IEEE J. Sel. Top. Quantum Electron.* **2010**, *16*, 1827–1837.
22. Liu, J. W.; Namboothiry, M. A. G.; Carroll, D. L. Optical Geometries for Fiber-Based Organic Photovoltaics. *Appl. Phys. Lett.* **2007**, *90*, 133515.
23. Li, G.; Zhu, R.; Yang, Y. Polymer Solar Cells. *Nat. Photonics* **2012**, *6*, 153–161.
24. He, Z.; Zhong, C.; Huang, X.; Wong, W.-Y.; Wu, H.; Chen, L.; Su, S.; Cao, Y. Simultaneous Enhancement of Open-Circuit Voltage, Short-Circuit Current Density, and Fill Factor in Polymer Solar Cells. *Adv. Mater.* **2011**, *23*, 4636–4643.
25. Dou, L. T.; You, J. B.; Yang, J.; Chen, C. C.; He, Y. J.; Murase, S.; Moriarty, T.; Emery, K.; Li, G.; Yang, Y. Tandem Polymer Solar Cells Featuring a Spectrally Matched Low-Bandgap Polymer. *Nat. Photonics* **2012**, *6*, 180–185.
26. Xia, X. Y.; Wang, S. S.; Jia, Y.; Bian, Z. Q.; Wu, D. H.; Zhang, L. H.; Cao, A. Y.; Huang, C. H. Infrared-Transparent Polymer Solar Cells. *J. Mater. Chem.* **2010**, *20*, 8478–8482.
27. Lee, Y. Y.; Tu, K. H.; Yu, C. C.; Li, S. S.; Hwang, J. Y.; Lin, C. C.; Chen, K. H.; Chen, L. C.; Chen, H. L.; Chen, C. W. Top Laminated Graphene Electrode in a Semitransparent Polymer Solar Cell by Simultaneous Thermal Annealing/Releasing Method. *ACS Nano* **2011**, *5*, 6564–6570.
28. Chen, C.-C.; Dou, L.; Zhu, R.; Chung, C.-H.; Song, T.-B.; Zheng, Y. B.; Hawks, S.; Li, G.; Weiss, P. S.; Yang, Y. Visibly

Transparent Polymer Solar Cells Produced by Solution Processing. *ACS Nano* **2012**, *6*, 7185–7190.
29. Liu, Z. K.; Li, J. H.; Sun, Z. H.; Tai, G. A.; Lau, S. P.; Yan, F. The Application of Highly Doped Single-Layer Graphene as the Top Electrodes of Semitransparent Organic Solar Cells. *ACS Nano* **2012**, *6*, 810–818.
30. Yang, Z.; Chen, T.; He, R.; Guan, G.; Li, H.; Qiu, L.; Peng, H. Aligned Carbon Nanotube Sheets for the Electrodes of Organic Solar Cells. *Adv. Mater.* **2011**, *23*, 5436–5439.
31. Zhang, S.; Ji, C.; Bian, Z.; Liu, R.; Xia, X.; Yun, D.; Zhang, L.; Huang, C.; Cao, A. Single-Wire Dye-Sensitized Solar Cells Wrapped by Carbon Nanotube Film Electrodes. *Nano Lett.* **2011**, *11*, 3383–3387.
32. Chen, T.; Qiu, L.; Cai, Z.; Gong, F.; Yang, Z.; Wang, Z.; Peng, H. Intertwined Aligned Carbon Nanotube Fiber Based Dye-Sensitized Solar Cells. *Nano Lett.* **2012**, *12*, 2568–2572.
33. Chen, T.; Qiu, L.; Kia, H. G.; Yang, Z.; Peng, H. Designing Aligned Inorganic Nanotubes at the Electrode Interface: Towards Highly Efficient Photovoltaic Wires. *Adv. Mater.* **2012**, *24*, 4623–4628.
34. Zhang, S.; Ji, C.; Bian, Z.; Yu, P.; Zhang, L.; Liu, D.; Shi, E.; Shang, Y.; Peng, H.; Cheng, Q.; *et al.* Porous, Platinum Nanoparticle-Adsorbed Carbon Nanotube Yarns for Efficient Fiber Solar Cells. *ACS Nano* **2012**, *6*, 7191–7198.